Translocation of an Intracellular Antigen to the Surface of Medullary Breast Cancer Cells Early in Apoptosis Allows for an Antigen-Driven Antibody Response Elicited by Tumor-Infiltrating B Cells[1]

Margit H. Hansen,[2] Heidi V. Nielsen,[2] and Henrik J. Ditzel[3]

Tumor-infiltrating lymphoplasmacytic cells are a key feature of medullary carcinoma of the breast (MCB), a distinct subtype of human breast cancer that, despite cytologically anaplastic characteristics, has a more favorable prognosis than other types of breast cancer. Since it has been proposed that the improved clinical outcome is due at least in part to the presence of a prominent lymphoplasmacytic cell infiltrate in the tumor stroma, we recently examined the tumor-infiltrating B cell response in MCB and showed that it is oligoclonal and directed against an intracellular protein translocated to the cell surface upon MCB cell apoptosis. Human Abs cloned from MCB lymphoplasmacytic infiltrate-derived phage display libraries and reflecting the dominant part of the response were used to identify the target Ag as actin. Here, we have characterized in detail the cloned human IgG Abs and the translocation process of actin to the cell surface of apoptotic MCB cells. Our analysis shows that the cloned Abs bind specifically and with high affinity to actin, as determined by ELISA and surface plasmon resonance. Sequence analysis revealed that the Abs are highly somatically mutated, with high replacement to silent ratios, indicative of an Ag-driven, affinity-matured response. Interestingly, the tumor-infiltrating B cells in half the MCB patients mainly exhibited an IgG2 response, while IgG1 dominated in the others. To gain insight to the molecular events that may elicit such an Ab response, we examined the translocation of actin to the cell surface of apoptotic MCB cells using flow cytometry and laser scanning cytometry. Our results show that actin becomes exposed on the cell surface of a large proportion of apoptotic MCB cells as an early apoptotic event. We propose that the Ab response against actin produced by tumor-infiltrating B lymphoplasmacytic cells is Ag-driven, affinity-matured, and elicited due to the increased rate of apoptosis occurring within the MCB tumor that facilitates the translocation and proteolytic fragmentation of intracellular proteins. *The Journal of Immunology*, **2002, 169: 2701–2711.**

Human breast cancers can be divided into histopathologic subtypes with distinct biological and prognostic characteristics. Among these, medullary carcinoma of the breast (MCB)[4] represents a minor morphologically and biologically distinct group (3–7% of breast cancer) that, despite cytologically anaplastic features, has a more favorable prognosis than other types of breast cancer at similar stages of differentiation. In multiple studies the 10-year survival of MCB patients has been ~84 vs 63% for ductal breast cancer patients (1–6). MCB is characterized by prominent lymphoplasmacytic infiltrates in the tumor stroma. In addition, the morphological criteria includes well-circumscribed tumor borders, syncytial growth pattern with absence of glandular pattern, large pleomorphic nucleoli, increased mitotic rate, sparse necrosis, and no tubular component. These diagnostic criteria for MCB were originally defined by Ridolfi et al. (3), but because their complexity led to high inter- and intraobserver variability, several groups have developed simplified definitions that have confirmed the prognostic importance and, in several cases, resulted in increased statistical survival in the MCB vs ductal carcinoma groups (1, 2, 6, 7). Importantly, these simplified definitions always included the histopathologic criteria of lymphoplasmacytic cell infiltrate, demonstrating its importance to the improved prognosis and suggesting that the host immune response is involved in restraining tumor growth.

The current understanding of the molecular basis for the specific morphological and prognostic characteristics of MCB is very limited; however, recent studies have demonstrated alterations in the p53 gene in nearly 100% of MCBs and immunohistochemically verified accumulation of p53 in the nuclei of tumor cells in MCBs (8–11). In comparison, p53 alterations are found in only 20–40% of invasive ductal breast cancers. MCB has also been found with high frequency among biopsy specimens from patients with BRCA1-associated breast cancer (12), a marker that otherwise is only found in hereditary breast cancer. Finally, a recent study showed that while >80% of invasive breast carcinomas lost the expression of secreted frizzled-related protein 1, a protein expressed in the epithelial component of normal breast and involved in the cancer-influenced WNT pathway, MCB maintain the normal expression level (13).

Several studies have analyzed the phenotypes of the lymphoplasmacytic cell infiltrate and demonstrated a predominance of cytotoxic $CD8^+$ T cells as well as large numbers of $CD4^+$ T, B, and

Department of Immunology, The Scripps Research Institute, La Jolla, CA 92037

Received for publication February 26, 2002. Accepted for publication July 3, 2002.

The costs of publication of this article were defrayed in part by the payment of page charges. This article must therefore be hereby marked *advertisement* in accordance with 18 U.S.C. Section 1734 solely to indicate this fact.

[1] This work was supported in part by grants from the California Breast Cancer Research Program (4JB-001) and the Danish Cancer Society.

[2] M.H.H. and H.V.N. contributed equally to this paper.

[3] Address correspondence and reprint requests to Dr. Henrik J. Ditzel, Department of Immunology, IMM2, The Scripps Research Institute, 10550 North Torrey Pines Road, La Jolla, CA 92037. E-mail address: hditzel@scripps.edu

[4] Abbreviations used in this paper: MCB, medullary carcinoma of the breast; CDR, complementarity-determining region; CHX, cycloheximide; FR, framework region; LSC, laser scanning cytometry; PI, propidium iodide; R/S ratio, replacement (R) to silent (S) mutation ratio.

0022-1767/02/$02.00

plasma cells (3). In contrast, no neutrophils were observed, indicating that the tumor-infiltrating leukocytes in MCB are not a nonspecific inflammatory response due to tumor necrosis or bacterial agents, but, rather, a result of specific stimuli. The Ig produced by the infiltrating plasma cells is predominantly of the IgG class, in contrast to IgA produced by plasma cells in normal breast glands (14). Analysis of MCB-infiltrating T cells identified a significant number of granzyme B-positive activated cytotoxic T cells, and in comparative studies the frequency of these cells in MCB was significantly higher than in poorly differentiated ductal carcinoma (15). Interestingly, granzyme B-positive activated cytotoxic T cells as well as plasma cells (16) were often located in close proximity to apoptotic MCB cells (15, 17), suggesting that in situ lymphoid proliferation is influenced by tumor-related stimuli. This lead us recently to attempt to identify the antigenic target of the dominant Ab response generated by these tumor-infiltrating cells. By analyzing the MCB-infiltrating B lymphoplasmacytic cells and the Abs produced by these cells at the molecular RNA and protein levels, we demonstrated that the dominant clones in the tumor-infiltrating response were directed against the cytoskeletal protein β-actin (18). We further showed that actin was exposed on the cell surface of MCB undergoing apoptosis, a frequent process in these tumors (8, 19, 20), and that actin was proteolytically cleaved by T cell-induced granzyme B. These findings suggest that the humoral immune response against the self-Ag actin is elicited as a result of MCB apoptosis induced by T cells and/or intrinsic biological features. Another recent study examined the Ab response of tumor-infiltrating lymphocytic cells in MCB (21). Although they were unable to identify the target Ag of the infiltrating B cell response, and thus could not specifically examine the Abs against the target Ag, they found, similar to our observation, that the Ab response in these tumors was oligoclonal and showed signs of an Ag-driven response.

In this study we extended the analysis of the oligoclonal response in MCB and analyzed in detailed the anti-actin Abs isolated from IgG phage display libraries generated from tumor-infiltrating B lymphoplasmacytic cells. We show that the anti-actin Abs are of high affinity, are highly specific for actin, and exhibit extensive somatic mutations and high replacement to silent ratios, all indicative of an Ag-driven, affinity-matured response. To gain insight into the molecular events inducing this response, we examined the translocation of actin to the cell surface of MCB using flow cytometry and laser scanning cytometry (LSC) and showed that actin is exposed on the surface of ~18% of apoptotic MCB cells as an early apoptotic event.

Materials and Methods

Patients

Formalin-fixed, paraffin-embedded tissue and fresh-frozen tissue from eight patients with typical MCB, as defined by Ridolfi et al. (3), were examined. All the MCBs had significant lymphoplasmacytic infiltration, but no other special clinicopathologic features and no metastasis or confounding medical conditions, such as infections. Human materials were obtained according to human subject protocol 99-105 approved by The Scripps Research Institute's human subjects committee.

Ig subclass determination

RNA was isolated from 0.5-cm^3 blocks of the lymphoplasmacytic-rich, fresh-frozen MCB tissue to ensure that representative material was obtained. Multiple sections were cut and immediately ground in guanidium chloride/ME to avoid RNA degradation. The isolated RNA was reverse transcribed, and the cDNA generated from the different MCB samples were used as a template for Ig class and subclass determinations. Constant region-specific primers (IgG1, IgG2, IgG3, IgG4, and IgA) combined individually with a mixture of the variable H chain (V_H) family primers (V_H135, V_H4, and V_H4b) (22) were used for amplification of IgG1, IgG2, IgG3, IgG4, and IgA genes, and the amplified products were separated by electrophoresis using gels made of 2% UltraPure agarose (Life Technologies, Grand Island, NY) and 2% NuSieve agarose (BioWhittaker Molecular Applicants, Rockland, ME).

Library construction and phage selection

RNA isolated from the MCB tissues containing the tumor-infiltrating B cells were also used as starting materials for library construction using the pComb3 and pComb3H M13 surface display systems as previously described (23). Specific Ab clones were selected from the phage libraries by panning on frozen tissue sections (24, 25). In brief, phage resuspended in PBS containing 1% BSA (Sigma-Aldrich, St. Louis, MO) were incubated for 2 h at room temperature. Unbound phage were removed by washing five times with PBS containing 1% BSA. Bound phage, enriched for those bearing Ag-binding surface Fabs, were eluted with 0.2 M glycine-HCl buffer, pH 2.2. The eluted phages were amplified by infection of *Escherichia coli* and superinfection with M13 helper phage. The panning procedure was repeated five times, after which phagemid DNA was prepared from the last round, and the gene III fragment was removed by treatment with the enzymes *Nhe*I and *Spe*I (New England Biolabs, Beverly, MA), followed by ligation. The reconstructed phagemid was used to transform XL1-Blue cells (Stratagene, La Jolla, CA) to produce clones secreting soluble Fabs.

Soluble Fab expression and ELISA analysis

Fabs were expressed in bacterial supernatants, as previously described, with minor modifications (23, 24). In brief, *E. coli* containing the appropriate clone was inoculated into liter cultures of superbroth containing carbenicillin (50 μg/ml), tetracycline (10 μg/ml), and $MgCl_2$ (20 mM) and grown at 37°C, with shaking, for 6 h. Protein expression was then induced with 2 mM isopropyl β-D-thiogalactopyranoside, and the cells were grown at 30°C overnight. The bacteria were pelleted by centrifugation, resuspended in PBS with 200 μM PMSF, and freeze-thawed four times. The Fab-containing bacterial supernatants were collected after removal of the cell debris by centrifugation 15,000 rpm for 30 min at 4°C and were used for the different binding analysis.

The concentration of Fab in the bacterial supernatants was determined with an anti-IgG Fab sandwich ELISA. The ELISA wells (Costar, Cambridge, MA) was coated with goat anti-human IgG $F(ab)_2$ Ab (5 μg/ml in PBS; Pierce, Rockford, IL) overnight at 4°C, washed three times with PBS, and blocked with 5% nonfat dry milk. Fab-containing supernatants in serial dilutions were incubated for 1 h at 37°C, followed by washing 10 times with PBS-0.05% Tween. Detection of bound human Fabs was conducted with alkaline phosphatase-labeled goat anti-human IgG $F(ab')_2$ Ab (Pierce) diluted 1/500 in PBS, and visualized with nitrophenol substrate (Sigma-Aldrich) by reading absorbance at 405 nm. The concentration of Fab in the preparations was determined by comparison with a standard curve generated from serial dilutions of a Fab with a known concentration run in parallel.

To assess specificity, supernatants were screened by ELISA against nonmuscle actin (2 μg/ml; Cytoskeleton, Denver, CO), muscle actin (2 μg/ml; Cytoskeleton), and a panel of unrelated Ags, including BSA (2 μg/ml; New England Biolabs), annexin V (2 μg/ml; Sigma), HIV-1 gp120 (2 μg/ml; Intracell, Issaquah, WA), Fc fragment of IgG (2 μg/ml; Jackson ImmunoResearch Laboratories, West Grove, PA), and DNA (10 μg/ml; Sigma-Aldrich). Human Fabs or mouse anti-actin Ab were incubated with the test Ag for 2 h at 37°C, followed by washing 10 times with PBS-0.05% Tween. Detection of bound Ab was conducted with alkaline phosphatase-labeled goat anti-human IgG $F(ab')_2$ Ab (Pierce) or alkaline phosphatase-labeled goat anti-mouse IgG Ab (Pierce) diluted 1/500 in PBS and visualized as described above.

Nucleic acid sequencing

Nucleic acid sequencing was conducted on a 373A automated DNA sequencer (PE Applied Biosystems, Foster City, CA) using a *Taq* fluorescent dideoxy terminator cycle sequencing kit (PE Applied Biosystems). Comparison to reported Ig germline sequences from GenBank and EMBL was performed using the Genetic Computer Group sequence analysis program.

Surface plasmon resonance to measure Fab binding affinities

The kinetics of Fab binding to actin were determined by surface plasmon resonance-based measurements using an instrument from Biacore (Piscataway, NJ). Purified actin at a concentration of 4 μg/ml in 10 mM acetate buffer, pH 4.0, was coupled to a CM5 sensor chip using *N*-hydroxysuccinimide/*N*-ethyl-*N'*-(3-dimethylaminopropyl) carbodiimide amine coupling chemistry. BSA, used as a negative control Ag, was coupled to a

CM5 sensor chip at a concentration of 10 μg/ml in 10 mM acetate buffer, pH 5.0. Typically, 300 resonance units were immobilized. The association and dissociation rate constants, k_{on} and k_{off}, were determined under a continuous flow rate of 10 μl/min using a range of concentrations (5–2500 nM) of Fabs as previously described (26). Association and dissociation constants were deduced from the kinetic data using Bioevaluation program version 3.1 (Biacore).

Cell culture

The human MCB cell line BrCaMz01, a gift from Prof. V. Möbus (Universitätsklinikum, Ulm, Germany) was grown as a monolayer in DMEM supplemented with 10% FCS (Tissue Culture Biologists, Tulane, CA), 1% nonessential amino acids, 1% L-glutamine, 1% sodium pyruvate, and 100 U/ml each of penicillin and streptomycin. The MCB cell line, MDA-MB-157, and the squamous carcinoma cell line HEp-2 (American Type Culture Collection, Manassas, VA) were maintained in RPMI 1640, 10% FCS, 1% glutamine, and 100 U/ml each of penicillin and streptomycin. The breast cancer cell line MCF-7 (American Type Culture Collection) was maintained in EMEM, 10% FCS, 1% nonessential amino acids, 1% L-glutamine, 1% sodium pyruvate, 1% HEPES, and 100 U/ml each of penicillin and streptomycin. All medium components were obtained from Life Technologies unless otherwise noted.

Apoptosis induction

Apoptosis was induced by incubating the cells with 100 ng/ml TNF-α (Upstate Biotechnology, Lake Placid, NY) and 1 μg/ml cycloheximide (CHX) for 3–15 h at 37°C in 5% CO_2. Apoptosis was also induced by treating cells with staurosporine (Sigma-Aldrich) at 5 μM for 3–15 h at 37°C in 5% CO_2. Staurosporine was dissolved in DMSO, and the final DMSO concentration in cultures was 0.2%. Control cells received 0.2% DMSO only. Apoptotic cells were detected by the TUNEL method using either the In Situ Cell Death Detection kit (Roche, Indianapolis, IN) according to the manufacturer's instructions, annexin V-FITC (BD PharMingen, San Diego, CA) staining of phosphatidyl serine exposed on the cell surface of apoptotic cells, or the APO-BRDU kit (Phoenix Flow Systems, San Diego, CA).

Cell were grown in culture flasks, and detached cells were collected from the culture medium and subsequently pooled with the cells that were detached by trypsinization (Life Technologies). To minimize trypsin-induced damage to the cells, the trypsin was neutralized by immediately adding soybean trypsin inhibitor (Sigma-Aldrich) after the cells had detached. The cells were washed three times with ice-cold PBS and resuspended in FACS buffer (HBSS (Life Technologies), 2% BSA (Sigma-Aldrich), and 25 mM HEPES (Life Technologies)).

Flow cytometry

BrCaMz01 cells resuspended in FACS buffer were incubated with mouse anti-actin Ab (clone C4; Roche) or control mAbs (M2 (Sigma-Aldrich), HA (Roche), p53 (Santa Cruz Biotechnology, Santa Cruz, CA)) for 30 min on ice. Cells were washed twice with PBS, resuspended in FACS buffer containing Cy5-conjugated goat $F(ab)_2$ anti-human IgG $F(ab)_2$ Ab (Jackson ImmunoResearch Laboratories), and incubated in ice for 30 min. In addition, cells were stained for apoptosis using FITC-labeled annexin V (BD PharMingen) and propidium iodide (PI; Sigma-Aldrich) according to the manufacturer's instructions. Flow cytometric data were acquired using a FACSCalibur or a FACS Sort flow cytometer (BD Biosciences, San Jose, CA), equipped with dual lasers. Data were collected and analyzed using CellQuest software (BD Biosciences).

LSC and immunocytochemical analysis using confocal laser scanning microscopy

Initially, data were collected by flow cytometry using a laser scanning cytometer from CompuCyte (Cambridge, MA), but additional single cells from selected gates were examined by the attached Olympus BX50 microscope (New Hyde Park, NY). Images of cells were generated by the CompuColor feature in the software and by a CCD camera. For confocal analysis of the apoptotic cells, incubation was performed in suspension as described above. Cells were fixed with ice-cold ethanol for 5 min, followed by four washes with PBS and blocking with 5% normal goat serum (BioSource International, Camarillo, CA) for 30 min. Fabs, diluted in PBS, were incubated for 1.5 h at room temperature. Fabs were detected using an FITC-labeled goat anti-human IgG $F(ab)_2$ (Jackson ImmunoResearch Laboratories) or Cy5-labeled goat $F(ab)_2$ anti-human IgG $F(ab)_2$ Ab (Jackson ImmunoResearch Laboratories). When appropriate, the cells were also incubated with FITC-labeled annexin V, and PI was added in the final step at 5 μg/ml for 10 min. Between all incubations, cells were washed five times for 3 min each time with PBS. The slides were mounted with Slow Fade in PBS/glycerol (Molecular Probes, Eugene, OR) before analysis using a Zeiss Axiovert S100 TV confocal microscope (New York, NY). As controls, all experiments were conducted omitting the primary Ab.

Immunohistochemical analysis

Fresh-frozen MCB tissue sections fixed in 96% ethanol for 5 min and incubated with the avidin/biotin blocking kit (Vector Laboratories, Burlingame, CA) were examined by a panel of lymphocytic markers including anti-CD8 (clones 4B11 and 1A5), anti-CD20 (clone L-26; all from Novocastra, Newcastle, U.K.), B lymphocyte Ag BLA.36, anti-CD3 (both from DAKO, Carpinteria, CA), and anti-cytokeratin 18 (CY-90; Sigma-Aldrich) to determine the cell type present in the mononuclear cell infiltrate as previously described (27). Bound Abs were visualized using the Elite Vectastain ABC kit (Vector Laboratories) and the liquid diaminobenzidene substrate kit (Zymed Laboratories, South San Francisco, CA). As controls, all experiments were conducted omitting the primary Ab.

Results

Characterization of the lymphoplasmacytic cell infiltrates in MCB

Initially, fresh-frozen tumor tissue from eight MCBs, all fulfilling the criteria of Ridolfi, were obtained, and the characteristics of the tumor mononuclear cell infiltration were examined using morphology and immunohistochemistry. All eight patients had good clinical outcome following surgery, with a minimum 7-year disease-free interval. As shown in Fig. 1, exemplified by one representative tumor, all eight MCBs exhibited significant diffuse lymphoplasmacytic infiltration containing significant numbers of T, B, and plasma cells, whereas no neutrophils were observed. The infiltrating T, B, and plasma cells were found in both the intratumoral stroma and within tumor cell nests, as observed by others (2, 15, 16).

The MCB-infiltrating Ab response is of the IgG1 and IgG2 subclass

Previous analysis of the Ig VDJ segments from the MCB-infiltrating lymphoplasmacytic cells showed that the B cell response was oligoclonal (18). To evaluate the Ig subclass distribution of this oligoclonal response, total cellular RNA isolated from each of the MCB tissues were reverse transcribed into cDNA and amplified by PCR using a panel of subclass-specific primers. Interestingly, the IgG2 subclass, which generally constitutes only a minor part of the Ab response, was responsible for a major part of the response in four of seven tumors, while in the others the IgG1 subclass dominated as expected. The three most different examples are shown in Fig. 2, including MCB RH-12 exhibiting IgG2 dominance; MCB N-21 exhibiting about equal dominance of IgG1, IgG2, and IgG3; and MCB N-1 exhibiting IgG1 dominance. In none of the MCB cDNA samples was IgA amplified, which is in distinct contrast to normal breast tissue, where IgA represents the major Ig class (28). Furthermore, the cDNA for IgG3 and IgG4 were only weakly amplified or were not amplified at all. No correlation between the dominance of a particular Ig subclass and the clinical parameters was observed.

MCB-infiltrating Abs specifically recognize actin

Using Ag purification and mass spectrometry we previously showed that the Ag of the dominant Ab response in MCB recognized actin. To examine whether the dominant MCB-reactive IgG Fabs cloned from the two tumor-infiltrating lymphoplasmacytic cell-derived phage display libraries were monospecific for actin, they were tested for binding to a panel of Ags, including rabbit skeletal muscle actin (which exhibits 100% homology with human skeletal muscle actin), non-muscle actin (isolated from human platelets, a mixture of β- and γ-actin), BSA, HIV-1 gp120, the Fc fragment of IgG, and annexin V by ELISA. As shown in Fig. 3,

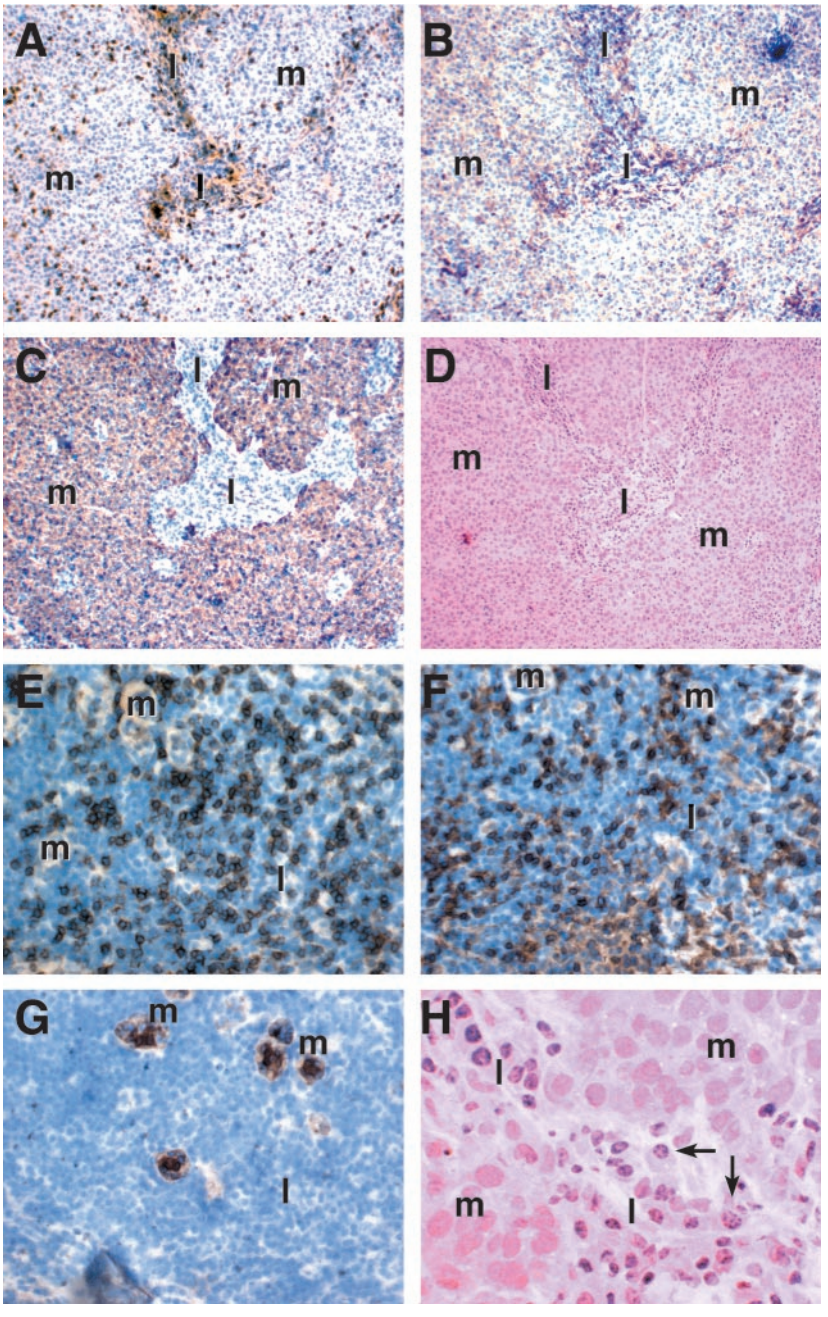

FIGURE 1. Immunohistochemical analysis of the lymphoplasmacytic cell infiltrate in MCB revealed pronounced diffuse infiltration of T, B, and plasma cells in intratumoral stroma and within tumor cell nests. Consecutive sections of fresh-frozen tissue of a representative MCB tumor were stained with a panel of leukocyte markers, including the CTL T cell marker CD8 (*A* and *E*) and the B cell marker BLA.36 (*B* and *F*; visualized using diaminobenzidene, brown stain). MCB cells (m), as opposed to lymphoplasmacytic-rich stromal tissue (l), were identified by staining sections with an anti-cytokeratin 18 Ab (*C* and *G*). The sections were counterstained with hematoxylin (blue stain). Plasma cells were identified based on their characteristic morphology on H&E-stained sections (*D* and *H*, arrows). Magnification: ×200 (*A–D*), ×400 (*E–G*), and ×500 (*H*).

Fabs HB21, HB24, RH49, RH87, and RH63 bound to non-muscle and muscle actins, but not to the other Ags, ruling out polyreactivity of the Fabs. Interestingly, the Fabs exhibited stronger reactivity with non-muscle than with muscle actin. Non-muscle actin and actin showed 94% homology, with a difference at the amino acid level in 25 positions. Several of the Fabs were also tested for binding to Western blots of MCB cell lysates and showed staining of only one band with the mobility of 43 kDa corresponding to actin (data not shown).

The RH-12 library was constructed in the pComb3 vector and the N-21 library in the pComb3H vector, which allowed us to verify that no cross-contamination had occurred during selection. Furthermore, the RH-12 Ab library was of the IgG2 subclass, and the N-21 library was of the IgG1 subclass, since the dominant responses of the two donor tumor-inflating responses were of the IgG2 and IgG1 subclasses, respectively. The library differences allowed us to verify that the specificity of the dominant clones in the tumor-infiltrating lymphoplasmacytic response of both MCB patients was truly against actin.

Nucleotide and amino acid analyses of anti-actin Abs isolated from the MCB-infiltrating lymphoplasmacytic cell-derived phage display libraries

We next examined whether the anti-actin IgG Abs isolated from the phage display libraries of two MCB patients exhibited signs of being evolved as a result of an Ag-driven response. The variable H and L chain genes of the anti-actin IgGs were compared with the closest germline sequences in the GenBank database. The deduced H chain amino acid sequences are shown in Fig. 4.

Because previous studies have shown that the Ab H chain is usually the major contributor to Ag binding (29), detailed analysis was focused on the H chain. All variable H chain region genes of the anti-actin IgGs were significantly mutated, with nucleotide and amino acid homologies to the closest germline in the range of

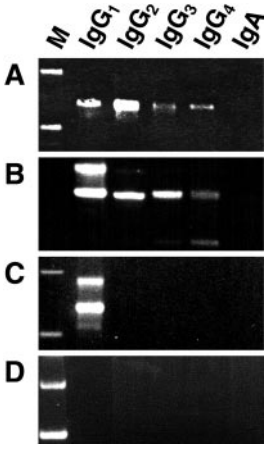

FIGURE 2. Ig subclass analysis of the MCB infiltrating Ab response, as determined by RT-PCR amplification with IgG and IgA subclass-specific primers. The Ig subclass analysis of cDNA of MCB-infiltrating B lymphoplasmacytic cells of RH-12 (*A*), N-21 (*B*), and N-1 (*C*) is shown. In addition, cDNA of a breast ductal carcinoma in which an immune response was not expected was included as a control (*D*). M, marker.

91–99% (average, 94%) and 86–99% (average, 93%), respectively, characteristic of an affinity-matured Ab response (Table I). All the anti-actin IgGs used germline genes of the dominant V_H1 and V_H3 families. The identification of the closest germline D segment proved difficult due to significant somatic modification, including N additions, deletions, and inversions. A wide panel of different D segments was used, and no obvious restriction was found (data not shown). Furthermore, the variable H chain genes exhibited a high replacement (R) to silent (S) mutation ratio (R/S ratio) for the complementarity-determining regions (CDR1 and -2) compared with the framework regions (FR1, -2, and -3; Table I). To probe for general trends in somatic mutation in the tumor-infiltrating Abs, we analyzed the amino acid replacement frequency (mutated amino acids/total amino acids) and the nucleotide replacement frequency (mutated nucleotides/total nucleotides) for the individual CDR and FR regions using published germline sequences (Fig. 5). The amino acid replacement frequencies of the different regions were: FR1, 3%; CDR1, 15%; FR2, 6.3%; CDR2, 16.8%; and FR3, 6.8%. Overall, these replacements are similar to those reported for circulating Ag-specific Abs (30–33).

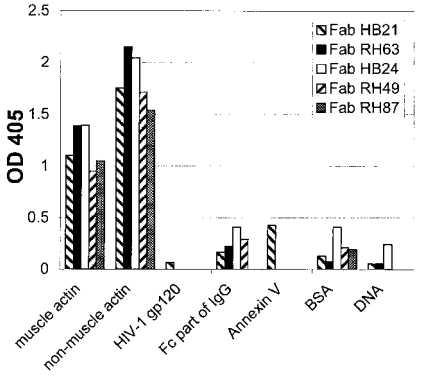

FIGURE 3. Specificity analysis of human IgG mAb Fabs shows strong binding to actin. The cloned anti-MCB IgG Fabs, representing the dominant clones in the tumor-infiltrating response, were tested for binding to muscle and non-muscle actin, BSA, HIV-1 gp120, human placental DNA, annexin V, and the Fc part of IgG by ELISA. The anti-HIV-1 gp120 Fab L17 (5 μg/ml), used as a control, bound to HIV-1 gp120, but not to actin or the other test Ags (data not shown).

Analysis of the clones isolated by tissue panning of the RH-12 IgG2 library showed that 9 of 21 had a similar H chain variable sequence (named the RH63), which was also identical with one of the dominating clones from the previous VDJ repertoire analysis used to evaluate oligoclonality. Interestingly, the RH63 sequence was not found among the 10 clones sequenced from the unselected RH-12 Ab library, indicating that amplification of this clone related to its Ag specificity and not to a bias in the library. When the H chain sequences of the RH63-like group of clones were analyzed in more detail, most contained nucleotide differences that, for six clones, also resulted in amino acid differences, indicating that the clones were somatic variants of one and another presumably evolved from a common ancestor. Further analysis of the pattern of the mutation allowed for generation of a genetic tree that demonstrated that the clones were probably derived from a common progenitor B cell through at least four rounds of division and differentiation (Fig. 6). Interestingly, the RH63 family had a three-amino acid insertion in the CDR1 compared with the closest germline gene $V_H3–49$. When the L chains of the six clones with the RH63-like H chain sequence were sequenced, all were completely different, and multiple variable L chain germline genes of both κ and λ were used (Fig. 7), demonstrating the importance of the RH63 H chain for binding to its Ag. The variable L chain region genes used were also significantly mutated, with nucleotide homologies to the closest germline in the range of 85–96%. In addition to the RH63 family, the clones HB49 and HB87 were repeatedly retrieved by selection of the RH-12 library, and both were identical with two of the dominant clones from the VDJ repertoire analysis. Detailed analysis of the clones with the HB49- and HB87-like sequences revealed no intraclonal variants, as observed for the RH63 family.

Analysis of the H chain variable sequence of the clones isolated by panning of the N-21 IgG1 library showed that four clones, HB21, HB24, HB28, and MC6, dominated and also represented the dominant part of the response as determined by the VDJ repertoire analysis. As observed for the RH-12 library, analysis of the H chain variable sequences of the HB21, HB28, and MC6 groups revealed multiple somatic variants (Fig. 4). In contrast to the RH63 family, where the clones seem to be derived from one progenitor cell, the members in the HB21 family seemed to derive from multiple progenitor cells that had converged to contain a common H chain CDR3 (Table I). While HB21 and hb130 used VH3–23 as closest germline gene, hb22 used VH3–11, and hb128 used VH1–69 as closest germline gene. With respect to the L variable genes, all four clones used the common Kv325 as closest germline gene (Fig. 7).

Fab affinity for actin

Abs of the IgG class involved in an active immune response generally exhibit high affinity for their autoantigen. Therefore, we next determined the kinetic constants for the interaction of selected anti-actin Fabs and actin by surface plasmon resonance. The K_d measured for Fabs RH63 and HB21 were 100 and 200 nM, respectively. Thus, the high degree of somatic mutation, the high R/S ratio, the intraclonal variants, and the affinity for the autoantigen indicate that these anti-actin IgG Abs are derived from MCB-infiltrating, B lymphoplasmacytic cells involved in an active immune response.

Actin becomes exposed on the cell surface of MCB cells at an early phase of apoptosis

Cancer cells undergo apoptosis at a higher frequency in MCB than other types of breast cancer (8, 19, 20), and we have shown by confocal microscopy that actin became exposed on the cell surface

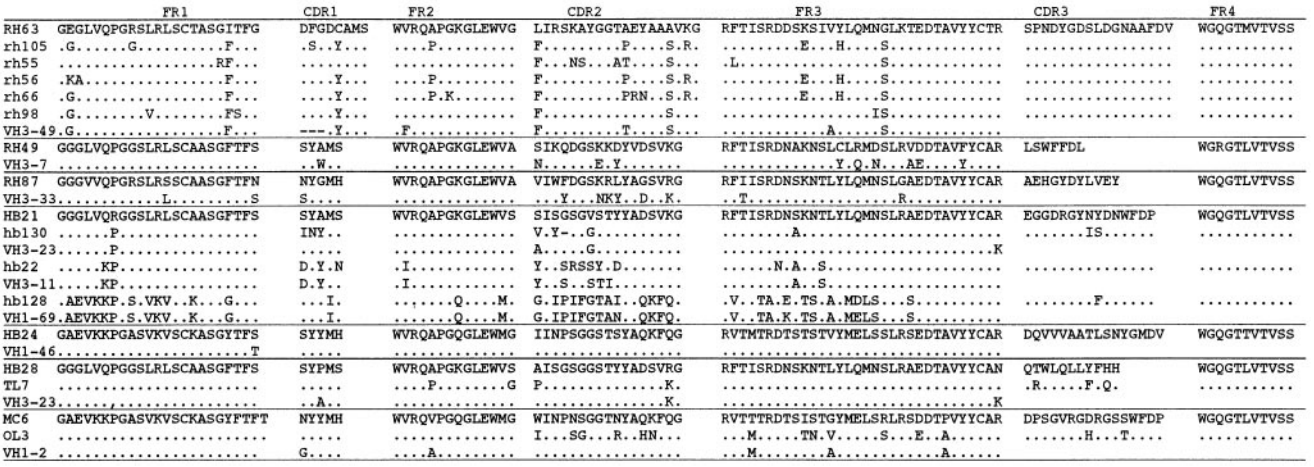

FIGURE 4. The anti-MCB IgG Abs cloned from tumor-infiltrating lymphoplasmacytic cells of two MCB patients are somatically mutated and exhibit high R/S ratios. Deduced amino acid sequences of the H chain variable (V_H) domains of the panel of anti-MCB Fabs are compared with the closest germline sequence. Identity with the first sequence in a group is indicated by dots. Short lines indicate an amino acid missing from the sequence compared the closest germline sequence.

of apoptotic MCB cells, suggesting a mechanism by which the humoral immune system would encounter this intracellular Ag and elicit a local immune response within the tumor. To obtain more quantitative data on the surface exposure of actin and to evaluate when in the apoptotic process actin becomes exposed, MCB cell cultures were analyzed by flow cytometry and laser scanning cytometry.

BrCaMz01 MCB cells induced with TNF-α and CHX to undergo apoptosis were initially processed as monolayers in chamber slides. However, since the cells undergoing apoptosis rounded and detached from the plastic surface during the staining procedure, this approach was not practical. MCB cell cultures induced to undergo apoptosis were instead processed in suspension, as described in *Materials and Methods*. BrCaMz01 MCB cells, either untreated (Fig. 8, *columns 3* and *4*) or committed to apoptosis after exposure to TNF-α/CHX (Fig. 8, *columns 1* and *2*), were simultaneously incubated with an anti-actin Ab (C4) or isotype-matched control Abs, FITC-labeled annexin V, and PI. The isotype-matched control Abs included an Ab against talin, a cytoplasmic protein found in MCB cells, an Ab against p53, and an Ab against a FLAG-tag. The anti-actin Ab and the isotope controls were detected with Cy5-labeled anti-mouse IgG Ab. PI was included in all the experiments to ensure the integrity of the membrane throughout the entire procedure by excluding the possibility that anti-actin Abs bound intracellular actin instead of cell surface-exposed molecules. Apoptotic cells were visualized by the binding of annexin V to phosphatidylserine on the cell surface and at the same time exclusion of the vital dye PI. In initial experiments apoptosis was also identified by staining for caspase-3 and by TUNEL. Good agreement was observed for the number apoptotic cells identified with the three techniques (data not shown).

In each flow cytometry experiment a first gate was set to include the whole population of intact cells (Fig. 8, *row 1*). Next, a second set of gates was set to include the apoptotic ($FITC^+/PI^-$) or the necrotic ($FITC^+/PI^+$) cell populations, respectively (Fig. 8, *row 2*). Interestingly, a small amount of BrCaMz01 MCB cells (2–3%)

Table I. *Comparison of the nucleotide and deduced amino acid sequences of the V_H domains of the cloned anti-actin IgG with the closest germline sequences demonstrates the frequency of silent and replacement mutations*[a]

Clone	Closest Germline	Amino Acid Homology (%)	Nucleotide Homology (%)	R/S Ratio FRs	R/S Ratio CDRs
RH63	VH3–49	91	92	5/3:1.7	4/2:2.0
rh105	VH3–49	92	92	6/4:1.5	2/1:2.0
rh55	VH3–49	92	92	5/1:4.0	3/3:3.0
rh56	VH3–49	91	93	7/4:1.8	2/1:2.0
rh66	VH3–49	90	93	7/2:3.5	5/1:5.0
rh98	VH3–49	94	93	5/2:2.5	1/1:1.0
RH49	VH3–7	89	93	6/4:1.5	5/2:2.5
RH87	VH3–33	89	95	3/0:>3.0	8/1:8.0
HB21	VH3–23	96	96	1/3:0.3	3/2:1.5
hb22	VH3–11	93	96	1/1:1.0	7/0:>7.0
hb128	VH1–69	96	96	2/2:1.0	1/4:0.3
hb130	VH3–23	94	97	1/8:1.3	7/2:3.5
HB24	VH1–46	99	99	1/1:1.0	0/0:0.0
HB28	VH3–23	96	96	1/1:1.0	2/0:>2.0
TL7	VH3–23	95	95	3/3:1.0	2/1:2.0
MC6	VH1–2	94	96	4/1:4.0	2/0:>2.0
OL3	VH1–2	86	91	6/5:1.2	11/3:3.7

[a] In addition, the percent homologies, in terms of nucleotide and amino acid sequence compared with the closest germline sequence, are shown.

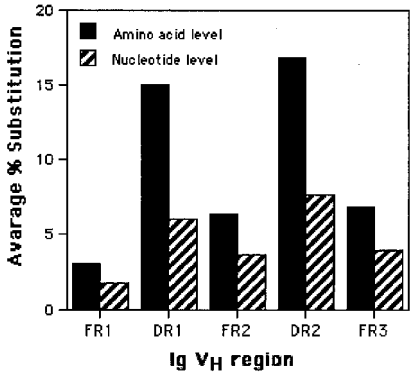

FIGURE 5. Analysis of the distribution of nucleotide and amino acid changes within the V_H segment of the 17 anti-actin IgG Abs compared with their closest germline sequences. The average percentage of mutation for individual regions (FR1, DR1, FR2, DR2, and FR3) was calculated as the number of changes divided by the total number of nucleotides for the region. Similarly, the average percentage of amino acid substitution for individual regions was calculated as the number of amino acid changes divided by the total number of amino acids for the region.

was found to be apoptotic even in noninduced cultures. When TNF-α/CHX was added to the culture, the fraction of apoptotic cells increased to 17–18%. The anti-actin Ab, C4 (Fig. 8, *row 3*), but not the isotype-matched control Abs, bound to the apoptotic cells. In contrast, live BrCaMz01 MCB cells were not stained with either the anti-actin Ab or the control Ab. In the apoptotic cell population 17.5% of the cells were stained with the anti-actin Abs (bright Cy5), as opposed to only 0.4% in the healthy cell population (Fig. 8, *row 4*). The anti-actin Ab, but not the control Abs, also bound to a fraction of the 2–3% of spontaneously apoptotic BrMzCa01 MCB cells from the untreated cell culture.

The MCB cell samples induced to undergo apoptosis were also analyzed by LSC. This method, in addition to collection of flow cytometry data, allows microscopic views of the individual cells in the different populations. Initially, data were collected by flow cytometry, and subsequently, cells from selected gates were viewed in the microscope. As shown in Fig. 9, the amount of actin accessible to binding by anti-actin Ab increased dramatically when binding of the apoptotic marker reached a certain threshold level, indicating that actin became exposed on the MCB cell surface at a particular (distinct) early stage of apoptosis. Images of cells collected in the $Cy5^+/FITC^+$ gate were generated by CompuColor, visualizing the locations of the blue and green stains. Images of cells from outside this gate appeared negative for both Cy5 and FITC, and only the PI stain was seen, indicating that only apoptotic cells reacted with the anti-actin Abs. To determine the cellular distribution of anti-actin Ab bound to apoptotic cells ($Cy5^+FITC^+PI^-$) in more detail, high resolution images were obtained by confocal laser scanning microscopy. These images confirmed that a significant number of apoptotic cells exhibited surface staining by the anti-actin Ab, as shown by the blue Cy5 stain (data not shown). In contrast, apoptotic cells incubated with the isotype-matched control Abs (anti-talin Ab or anti-FLAG Ab) exhibited no Cy5 staining. PI^+ necrotic cells exhibited cell surface staining with neither the anti-actin Ab nor annexin V. The analysis also showed that not all cells were apoptotic or necrotic, since completely unstained cells ($Cy5^-FITC^-PI^-$) were seen on the differential interference contrast microscopy image (data not shown).

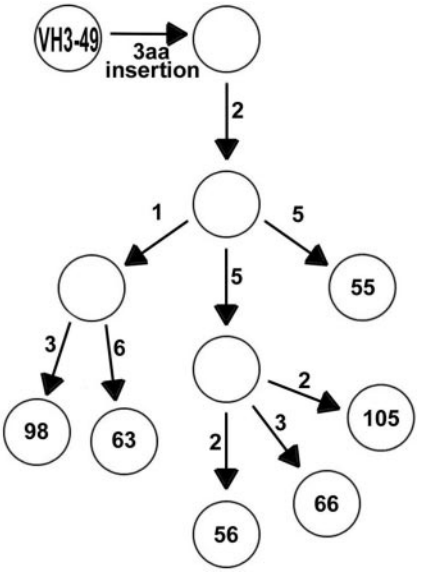

FIGURE 6. Genealogical tree demonstrating a possible clonal relationship between the MCB-infiltrating B lymphoplasmacytic cells within the RH63 family derived from the V_H3–49 germline. Numbers in the circles refer to the clone name, as also listed in Fig. 4. The circles without a number indicate deduced intermediates. Numbers next to arrows indicate the number of V_H gene amino acid changes between two clones. The tree was constructed according to the principle of minimizing the number of amino acid substitutions that occur twice in the tree.

Discussion

We analyzed the Ab repertoire produced by the tumor-infiltrating lymphoplasmacytic cells of MCB and examined the biological process that may allow such Ab repertoires to be elicited. Diffuse infiltration of lymphocytes, as seen in MCB, is also observed among a small number of other malignant solid tumors, including nasopharyngeal and gastric carcinomas, seminomas, and melanomas. Interestingly, the presence of such lymphoid infiltration within some of these malignant tissues has been correlated to a favorable prognosis (34, 35). This is particularly apparent for MCB, where a recent study found diffuse stromal infiltration of mononuclear cells as one of four histopathologic characteristics correlating to a better prognosis (36). Seven other histopathologic characteristics normally associated with MCB were not found to correlate with improved prognoses. Furthermore, risk factors such as lymph node status, invasion, steroid receptor status, and menopause, which are of major prognostic importance in breast cancer, had minimal prognostic value in MCB, indicating that MCB is a subtype with unique biological features (37). Because some form of immune surveillance seems to occur, the cell types of the MCB infiltrate have been intensely studied (15, 38–40). In addition, enhanced tumor cell apoptosis (8, 19, 20) and elevated levels of metastasis-inhibiting factors (8) or adhesion molecule ICAM-1 (38) have been suggested to influence the prognosis of MCB.

Generally, the role of the spontaneous immune response in controlling tumor growth and spread remains controversial. For most cancers, the immune system seems to have a limited effect, partially due to low immunogenicity and distortion of various effector functions of the infiltrating immune cells. However, detailed analysis of human tumor responses has led to the identification of a number of tumor-associated Ags that can be classified into categories according to their expression pattern, function, or origin: tumor-specific expressed Ags, differentiation Ags unique to a particular cell lineage, mutational Ags, and overexpressed self-Ags (41, 42). Spontaneous immune responses elicited by these Ags are either predominantly cellular, e.g., tyrosinase and Melan A/MART-1, or associated with a strong humoral immune component, e.g., NY-ESO-1 and p53 (42). The identification of these tumor-associated Ags

	FR1	CDR1	FR2	CDR2	FR3	CDR3	FR4
RH63	PLSLPVTPGEPASISC	ESSQGLLHSNGYISLN	WYLQKPGQSPQILIY	LGSNRAP	GVSDRFSGSGSGTDFTLKISTVEAEDVGIYYC	MQALQTPYT	FGQGTRLEVGR
rh105	.S..SASV.DRVT.T.	RA..SISSFLN	..Q....RA.KL...	AA.SLQS	..PS.....T.TSLQP..FAT...	Q.SYRN.AA	..G..KV.IK.
rh55	.DT.SLS...T.TL..	RA.HNINNRLN	..Q.....V.RLV.F	DS.Q.FH	TFPA.....NF..T.NSL.P..TAV...	Q.RSGW.PLT	..G...VDIK.
rh56	.PT.SLS...R.TL..	RA..S.SSFLA	..Q.....A.RL...	DA.K..T	DIPA.....F.....T..SL.PD..AV.F.	Q.RSNW.LT	..G..K..IR.
rh66	AP.VS.A...T.RIT.	GGNNIGSK.VN	..Q.....A.VLV..	YD...PS	.IPE.L...N..NTA..T..R...G.EAD...	QVWDSSSNHVV	..G..K.TVLG
rh98	.GT.SWS...R.TL..	RASRSVKSDSIA	..Q.....A.RL...	GA....T	.IPA.....T..SL.PD.FAV...	Q.SSGDVLT	..G.....IK.
HB21	PGTLSLSPGERATLSC	RASHSVSRAYLA	WYQQKPGQAPRLLIY	GTSSRAT	GIPDRFSGSGSGTDFTLTISRLEPEDFAVYYC	QQYGGSPW	FGQGTKVELKR
hb22	.....	...Q...SS...	.....	.A.....	.....A...	....N..PYT	......L.I..
hb128	.....	...Q...SS...	.....	.A.....	.....	....N..PYT	......L.I..
hb130	.....	...Q...SS...	.....	.A.....	.....A...	....A..ALT	..G.....I..

FIGURE 7. Deduced amino acid sequences of the L chain variable domains of the anti-MCB IgG Ab Fabs belonging to the RH63 or HB21 families. Identity with the first sequence in a group is indicated by dots.

indicates that at least some cancers are immunogenic, capable of eliciting limited humoral and cellular responses. In addition, circulating autoantibodies against several self-Ags have been described in patients with different cancers (43–45). The nature of such autoantibody responses, including whether they directly relate to the cancer process and/or represent major specificities in the Ab responses, is relatively

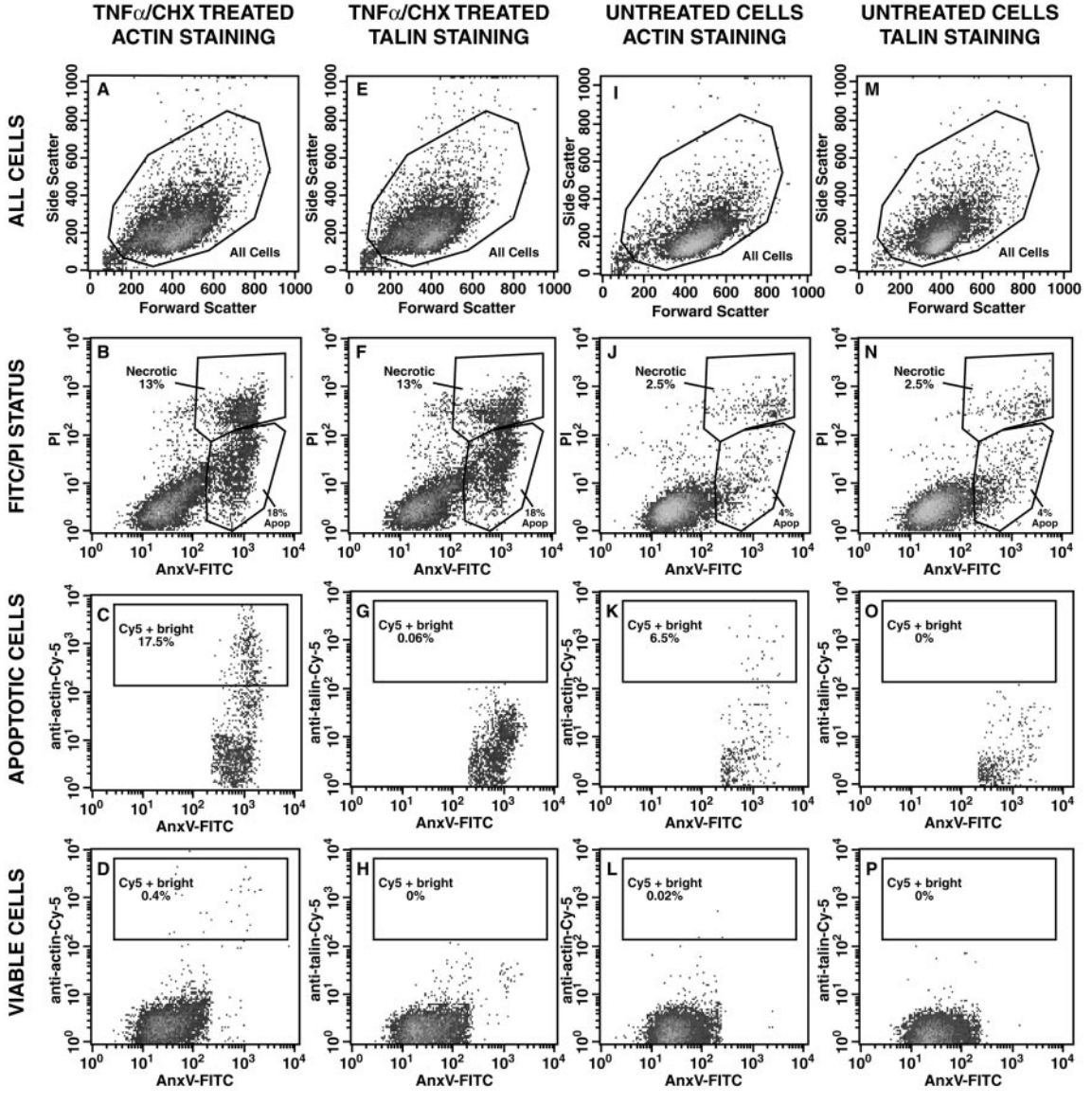

FIGURE 8. BrCaMz01 MCB cells, either untreated (*columns 3* and *4*) or committed to apoptosis after exposure to TNF-α and cycloheximide (*columns 1* and *2*), were stained with a Cy5-labeled anti-actin Ab (C4) or isotype-matched control Ab (directed against talin, a cytoplasmic Ag found in MCB cells), FITC-labeled annexin V, and PI and analyzed by flow cytometry, as described in *Materials and Methods*. Apoptotic, but not living, cells express phosphatidylserine, as demonstrated by staining with FITC-labeled annexin V. PI, which stains DNA, was added to the cells to ensure cell surface membrane integrity. Live cells and apoptotic cells have an intact cell surface membrane and do not exhibit nuclear staining with PI, whereas necrotic cells do. Of the intact cells (*row 1*) gates were set on apoptotic ($FITC^+PI^-$) and necrotic ($FITC^+PI^+$) cells (*row 2*). The anti-actin Ab, C4 (*y*-axis, *row 3*), but not an isotype-matched control Ab, bound to the apoptotic cells. In contrast, live BrCaMz01 MCB cells were not stained by either the anti-actin Ab or the control Ab. In the untreated BrMzCa01 MCB cells, 2.5% of the cells were apoptotic and bound the anti-actin Ab, but not the control Ab.

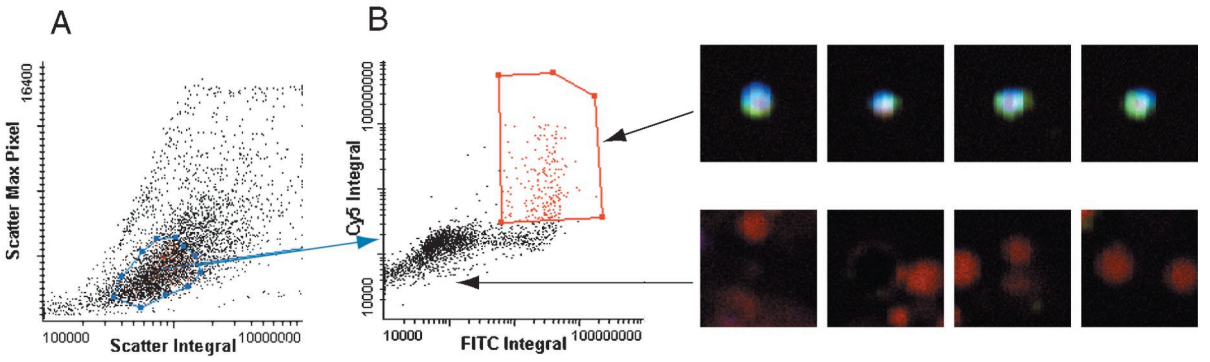

FIGURE 9. Analysis of actin cell surface staining on apoptotic MCB cells by laser scanning cytometry. *A*, A significant increase in anti-actin Ab binding was observed when the FITC signal (annexin V binding) reached a certain threshold. CompuColor images of single cells collected in the $Cy5^+/FITC^+$ gate demonstrated surface staining of the anti-actin Ab (blue stain) and annexin V (green stain), and no nuclear staining with PI (red stain). Similar images of cells from outside this gate exhibited no staining of the anti-actin Ab and annexin V, while only the PI stain was seen, indicating that only apoptotic, and not necrotic, cells exhibited cell surface binding by the anti-actin Ab.

unknown. To date, most studies have only analyzed crude sera for their binding analysis, and the Abs of interest have not been purified or cloned, which would allow more detailed characterization, such as affinity and specificity measurements (43–45). Our study used phage display to clone and express the Ab response and tissue selection to identify the dominant clones, which were subsequently used as probes to identify the major specificity of the response. Surprisingly, the specificity was found to be the self-Ag, β-actin, which is prevalent in most cells, rather than a tumor-specific molecule. Two Ab libraries were generated, each using RNA isolated from a large part of the whole tumor of an individual MCB patient as starting material. However, only the H chain variable chain genes of the B cells/plasma cells that had been Ig switched to IgG were amplified and used for the library construction. Since plasma cells contain 1000 times more mRNA encoding Ig than resting B cells, and our analysis showed that many plasma cells were present in the MCB tumors used, it seems likely that the major part of the library repertoire derives from plasma cells, while a minor part derives from activated IgG-switched B cells. Previous work with IgG phage display libraries generated from bone marrow of patients has shown that high affinity Abs with a given specificity are only isolated from relatively small immune libraries similar to that generated here, if the donor has reasonable numbers of specific plasma/B cells and corresponding serum Abs with the given specificity. Similar Abs were not isolated from seronegative donor libraries, demonstrating the importance of the immunization process (24, 46, 47). In addition, competition between the selected phage display Abs and the serum of the donor verified cloning of the major specificities of the serum response (48). These data allow us to be confident that the cloned anti-actin specificities reflect those synthesized in vivo by these tumor-infiltrating plasma cells in MCB rather than being an artifact generated by recombination of the Ig H and L chains.

Substantial evidence also supports the concept that anti-actin Abs represent the major Ab response in MCB and not simply a minor specificity isolated due to the high expression level of actin in both cancer cells and connective tissue. The selected anti-actin Abs, although not dominating the Ab libraries, represented the dominant clones in the immune response, as determined by VDJ sequence analysis (18). In addition, all selected Ab clones retrieved from the two MCB patients exhibited similar cytoplasmic staining patterns and actin reactivities. Since the two Ab libraries generated from the two MCB patients were of different Ig subclasses and generated in two different vectors (allowing them to be clearly distinguished by their electrophoresis band sizes following vector excision of the gene III), we are certain that the selected anti-actin clones were not the result of cross-contamination between the libraries. Finally, that the anti-actin response is Ag driven was shown by the presence of multiple Ab clones that were somatic variants of one and another, by significantly variable region mutation compared with the closest germline sequence, and by a high R/S ratio.

Generally, actin is relatively nonimmunogenic, and it is very difficult to generate mouse mAbs against actin, since an Ab response is not raised in the mice by standard immunization procedures (49). In addition, autoimmune patients with autoantibodies to a variety of autoantigens seldom have Abs against actin, with the exception of some patients with type 1 autoimmune hepatitis (50, 51). In these cited studies, anti-actin Abs were not present in a large panel of sera from patients with ductal breast adenocarcinoma (50, 51). Our previous findings suggested that the cause of the immune response against the intracellular protein actin in MCB relates to the increased rate of MCB cell apoptosis within the tumors; however, little was known about the quantitative and spaciotemporal parameters of this process (8, 18–20). Annexin V binding due to loss of membrane asymmetry and cell surface exposure of phosphatidylserine has been found to be an early event of apoptosis and precedes both characteristic morphological changes, nuclear condensation and DNA fragmentation (52, 53). Interestingly, our laser scanning cytometric analysis showed that actin became exposed on the cell surface at a distinct phase in the apoptotic process and at a time point where annexin V had intermediate intensity and had not yet reached a maximum signal. This indicates that the actin exposure is a relatively early apoptotic phenomenon that occurs at the so-called execution phase. In addition, flow cytometric analysis allowed us to quantify the frequency of apoptotic MCB cells expressing actin on the cell surface and demonstrated that ~18% of annexin V^+PI^- cells had actin exposed on the cell surface. In agreement with these observations, actin has been shown to accumulate at the periphery of apoptotic blebs early during the apoptotic process and to play an essential role in the different morphological changes occurring during apoptosis (54–56).

There are at least two possible explanations for the increased rate of apoptosis in MCB vs other breast cancers. MCB cell apoptosis may be caused by CTLs and/or by intrinsic biologic features that distinguish MCB cells from other breast cancer cells and render them more susceptible to apoptosis. As in other cancers with mononuclear cell infiltrates, such as EBV-associated gastric cancer and cervical, colorectal, and ductal breast carcinomas, the predominant phenotype of the tumor-infiltrating T lymphocytes in MCB is $CD8^+$ (57). However, an increased fraction of these CTLs was

found to be activated in MCB compared with ductal breast carcinomas (16, 40). Interestingly, a higher percentage of MCB cells express MHC classes I and II, and the average expression levels are higher than on infiltrating ductal carcinoma cells, allowing more effective tumor Ag presentation (39).

MCB cells form syncytia or giant cells with multiple nuclei. Such syncytia are normally observed only after infection with certain viruses, such as EBV, but no virus has been isolated from MCB cells to date (15). The loss of E-cadherin expression, a transmembrane protein and a prominent factor in maintaining the epithelial architectural structure, has been found to be significantly associated with the syncytial growth pattern (58). Interestingly, the cytoplasmic domain of E-cadherin is closely connected to the actin skeleton network via a complex of α-, β-, and γ-catenins (59, 60). An association between BCRA1 germline mutation and syncytial growth has also been observed (61, 62). It seems likely that several factors influence syncytial growth, and both BCRA1 and E-cadherin play important, but not exclusive, roles (58). Syncytial cells with fused and subsequently obliterated cell surface membranes may be more unstable and more susceptible to apoptosis.

Interestingly, we also found actin (18), similar to certain other autoantigens (63, 64), to be uniquely cleaved by the LAK- and CTL-specific protease, granzyme B, and found these actin fragments in MCB tissue, suggesting that CTLs play an important role in the MCB apoptotic process. It seems likely that the surface exposure of actin, either as aggregates or fragmented molecules, in the context of other apoptotic proteins, may render actin immunogenic. Similarly, other investigators have identified other intracellular Ags that were also exposed on surface blebs of apoptotic cells and elicited autoantibodies (65–67). Multiple factors other than apoptotic presentation of intracellular Ags, such as particular cytokine profiles and APC, are probably required for development of the anti-actin Ab response.

Several studies have found a correlation between poor prognosis of cancers and autoantibody levels (68–72). In breast cancer, particular interest in such correlations has focused on anti-53 autoantibodies, where some studies observed a correlation between poor prognosis and increased levels of anti-53 autoantibodies (70, 71), although these results could not always be confirmed by others (72). It may, therefore, seem surprising that the favorable prognosis of MCB correlates with anti-actin autoantibodies. A likely explanation is that different biological processes may lead to autoantibody production. Autoantibodies observed in some tumors may be due to large tumor masses and necrosis exposing a large amount of autoantigen to the immune system. Alternatively, as suggested for p53, in which mutations have been found to be associated with more aggressive tumors and poorer prognosis of breast cancer, the mutated p53 tends to have a much longer half-life than the wild-type p53, leading to accumulation of the protein and anti-p53 Ab production (70, 71). In contrast, the anti-actin Abs observed in MCB are probably a result of increased tumor cell apoptosis; thus, these Abs serve as a marker of a beneficial biologic process.

In summary, our study shows that the Abs derived from the oligoclonal B lymphoplasmacytic cells in MCB are generated as a result of an Ag-driven, affinity-matured IgG response against actin as a result of subcellular translocation and protein fragmentation. Detailed analysis of the translocation of actin to the cell surface of MCB showed that actin is exposed on the surface of ~18% of apoptotic MCB cells as an early apoptotic event and support the concept that the major portion of autoantibodies is elicited as a result of the perturbed state of apoptosis in cancer and autoimmune disease. As indicated above, the anti-actin IgG autoantibodies observed are most likely not directly responsible for the favorable prognosis, but result from T cell-mediated apoptosis of MCB cells and/or intrinsic biological features of MCB cells, thus serving as a marker of the pathogenic process. Further elucidation of the cellular arm of the immune response in MCB and the biological features intrinsic to these cancer cells, presumably also partially responsible for the increased apoptotic rate, should give clues to the favorable prognosis of MCB.

References

1. Wargotz, E. S., and S. G. Silverberg. 1988. Medullary carcinoma of the breast: a clinicopathologic study with appraisal of current diagnostic criteria. *Hum. Pathol. 19:1340.*
2. Jensen, M. L., H. Kiaer, J. Andersen, V. Jensen, and F. Melsen. 1997. Prognostic comparison of three classifications for medullary carcinomas of the breast. *Histopathology 30:523.*
3. Ridolfi, R. L., P. P. Rosen, A. Port, D. Kinne, and V. Mike. 1977. Medullary carcinoma of the breast. *Cancer 40:1365.*
4. Rapin, V., G. Contesso, H. I. Mouriesse, F. Bertin, M. J. Lacombe, J. D. Piekarski, J. P. Travagli, C. Gadenne, and S. Friedman. 1988. Medullary breast carcinoma: a revaluation of 95 cases of breast cancer with inflammatory stroma. *Cancer 61:2503.*
5. Reinfuss, M., A. Stelmach, J. Mitus, J. Rys, and K. Duda. 1995. Typical medullary carcinoma of the breast: a clinical and pathological analysis of 52 cases. *J. Surg. Oncol. 60:89.*
6. Pedersen, L., K. Zedeler, S. Holck, T. Schiødt, and H. T. Mouridsen. 1991. Medullary carcinoma of the breast, proposal for a new simplified histopathological definition. *Br. J. Cancer 63:591.*
7. Ellis, I. O., M. Galea, N. Broughton, A. Locker, R. W. Blamey, and C. W. Elston. 1992. Pathological prognostic factors in breast cancer. II. Histological type: relationship with survival in a large study with long-term follow-up. *Histopathlogy 20:479.*
8. Jensen, V., M. L. Jensen, H. Kiaer, J. Andersen, and F. Melsen. 1997. MIB-1 expression in breast carcinomas with medullary features: an immunohistological study including correlations with p53 and bcl-2. *Virchows Arch. 431:125.*
9. Domagala, W., B. Harezga, A. Szadowska, M. Markiewski, K. Weber, and M. Osborn. 1993. Nuclear p53 protein accumulates preferentially in medullary and high-grade ductal but rarely in lobular breast carcinomas. *Am. J. Pathol. 142:669.*
10. Marchetti, A., F. Buttitta, S. Pellegrini, F. Diella, D. Campani, D. Cecchetti, R. Callahan, and M. Bistocchi. 1993. p53 mutations and histological type of invasive breast carcinoma. *Cancer Res. 53:4665.*
11. de Cremoux, P., A. V. Salomon, S. Liva, R. Sendale, B. Bouchind'homme, E. Martin, and X. Sastre-Garau. 1999. p53 mutation as a genetic trait of typical medullary breast carcinoma. *J. Natl. Cancer Inst. 91:641.*
12. Eisinger, F., J. Jacquemier, C. Charpin, D. Stoppa-Lyonnet, B. Bressac-de Paillerets, J. P. Peyrat, M. Longy, J. M. Guinebretiere, R. Sauvan, T. Noguchi, et al. 1998. Mutations at BRCA1: the medullary breast carcinoma revisited. *Cancer Res. 58:1588.*
13. Ugolini, F., E. Charafe-Jauffret, V. J. Bardou, J. Geneix, J. Adélaïde, F. Labat-Moleur, F. Penault-Llorca, M. Longy, J. Jacquemier, D. Birnbaum, et al. 2001. WNT pathway and mammary carcinogenesis: loss of expression of candidate tumor suppressor gene SFRP1 in most invasive carcinomas except of the medullary type. *Oncogene 20:5810.*
14. Ito, T., S. Saga, S. Nagayoshi, M. Imai, A. Aoyama, T. Yokoi, and M. Hoshino. 1986. Class distribution of immunoglobulin-containing plasma cells in the stroma of medullary carcinoma of breast. *Breast Cancer Res. Treat. 7:97.*
15. Gaffey, M. J., H. F. Frierson, S. E. Mills, J. C. Boyd, R. J. Zarbo, J. F. Simpson, L. K. Gross, and L. M. Weiss. 1993. Medullary carcinoma of the breast: identification of lymphocyte subpopulations and their significance. *Mod. Pathol. 6:721.*
16. Yakirevich, E., O. B. Izhak, G. Rennert, Z. G. Kovacs, and M. B. Resnick. 1999. Cytotoxic phenotype of tumor infiltrating lymphocytes in medullary carcinoma of the breast. *Mod. Pathol. 12:1050.*
17. Jacquemier, J., L. Piana, M. Torrente, and J. Hassoun. 1987. Immunohistochemical study of T and B lymphocytes in human breast carcinomas with inflammatory stroma. *Breast Cancer 2:212.*
18. Hansen, M. H., H. Nielsen, and H. J. Ditzel. 2001. The tumor filtrating B cell response in medullary breast cancer is oligoclonal and directed against an intracellular antigen exposed on the surface of apoptotic cancer cells. *Proc. Natl. Acad. Sci. USA 98:12659.*
19. Kajiwara, M., S. Toyoshima, T. Yao, M. Tanaka, and M. Tsuneyoshi. 1999. Apoptosis and cell proliferation in medullary carcinoma of the breast: a comparative study between medullary and non-medullary carcinoma using the TUNEL method and immunohistochemistry. *J. Surg. Oncol. 70:209.*
20. Yakirevich, E., L. Maroun, O. Cohen, O. B. Izhak, G. Rennert, and M. B. Resnick. 2000. Apoptosis, proliferation, and Fas (APO-1, CD95)/Fas ligand expression in medullary carcinoma of the breast. *J. Pathol. 192:166.*
21. Coronella, J. A., P. Telleman, G. A. Kingsbury, T. D. Truong, S. Hays, and R. P. Junghans. 2001. Evidence for an antigen-driven humoral immune response in medullary ductal breast cancer. *Cancer Res. 61:7889.*
22. Glamann, J., D. R. Burton, P. W. H. I. Parren, H. J. Ditzel, K. A. Kent, C. Arnold, D. Montefiori, and V. M. Hirsch. 1998. Simian immunodeficiency virus (SIV) envelope-specific Fabs with high-level homologous neutralizing activity: recovery from a long-term-nonprogressor SIV-infected macaque. *J. Virol. 72:585.*
23. Burton, D. R., C. F. Barbas III, M. A. A. Persson, S. Koenig, R. M. Chanock, and R. A. Lerner. 1991. A large array of human monoclonal antibodies to type 1 human immunodeficiency virus from combinatorial libraries of asymptomatic seropositive individuals. *Proc. Natl. Acad. Sci. USA 88:10134.*
24. Ditzel, H. J., J. M. Binley, J. P. Moore, J. Sodroski, N. Sullivan, L. S. W. Sawyer, R. M. Hendry, W. P. Yang, C. F. Barbas III, and D. R. Burton. 1995. Neutralizing

recombinant human antibodies to a conformational V2- and CD4-binding site-sensitive epitope of HIV-1 gp120 isolated by using an epitope-masking procedure. *J. Immunol. 154:893.*
25. Ditzel, H. J., Y. Masaki, H. Nielsen, L. Farnes, and D. B. Burton. 2000. Cloning and expression of a novel human antibody-antigen pair associated with Felty's syndrome. *Proc. Natl. Acad. Sci. USA 97:9234.*
26. Karlsson, R. A., A. Michaelsson, and L. Mattsson. 1991. Kinetic analysis of monoclonal antibody-antigen interactions with a new biosensor based analytical system. *J. Immunol. Methods 145:229.*
27. Ditzel, H., K. Erb, P. Borup-Christensen, B. Nielsen, and J. C. Jensenius. 1991. Evaluation of prodecures for the fixation and processing of human tissue for immunohistochemical analysis of human monoclonal antibodies. *Hum. Antibody Hybridomas 2:135.*
28. Drife, J. O., D. B. McClelland, A. Pryde, M. M. Roberts, and I. I. Smith. 1976. Immunoglobulin synthesis in the "resting" breast. *Br. Med. J. 2:503.*
29. Burton, D. R., and C. F. Barbas III. 1994. Human antibodies from combinatorial libraries. *Adv. Immunol. 57:191.*
30. van Es, J. H., F. H. Gmelig Meyling, W. R. van de Akker, H. Aanstoot, R. H. Derksen, and T. Logtenberg. 1991. Somatic mutations in variable regions of human IgG anti-double-stranded DNA autoantibody suggest a role for antigen in induction of systemic lupus erythematosus. *J. Exp. Med. 173:461.*
31. Mantovani, L., R. L. Wilder, and P. Casali. 1993. Human rhematoid B-1a ($CD5^+$) cells make somatically hypermutated high affinity IgM rhematoid factors. *J. Immunol. 151:473.*
32. Ikematsu, H., N. Harindranath, Y. Ueki, A. L. Notkins, and P. Casali. 1993. Clonal analysis of a human antibody response. II. Sequences of the V_H genes of human monoclonal IgM, IgG, and IgA to rabies virus reveal preferential utilization of V_HIII segments and somatic hypermutation. *J. Immunol. 150:1325.*
33. Ikematsu, H., E. W. Schettino, M. Nakamura, and P. Casali. 1994. VH and VL segment structure of anti-insulin IgG autoantibodies in patients with insulin-dependent diabetes mellitus: evidence for somatic selection. *J. Immunol. 152:1430.*
34. Balch, C. M., L. B. Riley, Y. J. Bae, M. A. Sameron, C. D. Platsoucas, and A. Von Eschenbach. 1990. Patterns of human tumor infiltrating lymphocytes in 120 human cancers. *Arch. Surg. 125:200.*
35. Ben-Enza, J., and K. Sheibani. 1987. Antigenic phenotype of the lymphocytic component of medullary carcinoma of the breast. *Cancer 59:2037.*
36. Pedersen, L., S. Holck, T. Schiødt, K. Zedeler, and H. T. Mouridsen. 1994. Medullary carcinoma of the breast, prognostic importance of characteristic histopathological features evaluated in a multivariate Cox analysis. *Eur. J. Cancer 30A*:1792.
37. Pedersen, L., K. Zedeler, S. Holck, T. Schiødt, and H. T. Mouridsen. 1995. Medullary carcinoma of the breast: prevalence and prognostic importance of classical risk factors in breast cancer. *Eur. J. Cancer 312A:2289.*
38. Bacus, S. S., C. R. Zelnick, D. M. Chin, Y. Yarden, D. B. Kaminsky, J. Bennington, D. Wen, J. N. Marcus, and D. L. Page. 1994. Medullary carcinoma is associated with expression of intracellular adhesion molecule-1: implication to its morphology and its clinical behavior. *Am. J. Pathol. 145:1337.*
39. Feinmesser, M., A. Sulkes, S. Morgenstern, J. Sulkes, S. Stern, and E. Okon. 2000. HLA-DR and β_2 microglobulin expression in medullary and atypical medullary carcinoma of the breast: histopathologically similar but biologically distinct entities. *J. Clin. Pathol. 53:286.*
40. Tanaka, H., M. Hori, and T. Ohki. 1992. High endothelial venule and immunocomponent cells in typical medullary carcinoma of the breast. *Virchows Arch. 420:253.*
41. Soussi, T. 2000. p53 antibodies in the sera of patients with various types of cancer: a review. *Cancer Res. 60:1777.*
42. Boon, T., and L. J. Old. 1997. Cancer tumor antigens. *Curr. Opin. Immunol. 9:681.*
43. Lennon, G., and C. Auffray. 1996. The I.M.A.G.E. consortium: an integrated molecular analysis of genomes and their expression. *Genomics 33:151.*
44. Fernandez-Madrid, F., P. J. VandeVord, X. Yang, R. L. Karvonen, P. M. Simpson, M. J. Kraut, J. L. Granda, and J. E. Tomkiel. 1999. Antinuclear antibodies as potential markers of lung cancer. *Clin. Cancer Res. 5:1393.*
45. Vainio, E., G. M. Lenoir, and R. M. Franklin. 1983. Autoantibodies in three populations of Burkitt's lymphoma patients. *Clin. Exp. Immunol. 54:387.*
46. Barbas, C. F., III, T. A. Collet, W. Amberg, P. Roben, J. M. Binley, D. Hoekstra, D. Cababa, T. M. Jones, R. A. Williamson, G. R. Pilkington, et al. 1993. Molecular profile of an antibody response to HIV-1 as probed by combinatorial libraries. *J. Mol. Biol. 230:812.*
47. Barbas, S., H. J. Ditzel, E. M. Salonen, W. P. Yang, G. J. Silverman, and D. R. Burton. 1995. Human autoantibody recognition of DNA. *Proc. Natl. Acad. Sci. USA 92:2529.*
48. Graus, Y. F., J. J. Verschuuren, A. Degenhardt, P. J. van Breda Vriesman, M. H. de Baets, J. B. Posner, D. R. Burton, and J. Dalmau. 1998. Selection of recombinant anti-HuD Fab fragments from a phage display antibody library of a lung cancer patient with paraneoplastic encephalomyelitis. *J. Neuroimmunol. 82:200.*
49. Sheth, B., P. Banks, D. R. Burton, and P. N. Monk. 1991. The regulation of actin polymerization in differentiating U937 cells correlates with increased membrane levels of the pertussis-toxin-sensitive G-protein G_{i2}. *Biochem. J. 275:809.*
50. Czaja, A. J., F. Cassani, M. Cataleta, P. Valentini, and F. B. Bianchi. 1996. Frequency and significance of antibodies to actin in type 1 autoimmune hepatitis. *Hepatology 24:1068.*
51. Leibovitch, L., J. George, Y. Levi, R. Bakimer, and Y. Shoenfeld. 1995. Anti-actin antibodies in sera from patients with autoimmune liver diseases and patients with carcinomas by ELISA. *Immunol. Lett. 48:129.*
52. Martin, S. J., C. P. Reutelingsperger, A. J. McGahon, J. A. Rader, R. C. van Schie, D. M. LaFace, and D. R. Green. 1995. Early redistribution of plasma membrane phosphatidylserine is a general feature of apoptosis regardless of the initiating stimulus: inhibition by overexpression of Bcl-2 and Abl. *J. Exp. Med. 182:1545.*
53. van Engeland, M., L. J. Nieland, F. C. Ramaekers, B. Schutte, and C. P. Reutelingsperger. 1998. Annexin V-affinity assay: a review on an apoptosis detection system based on phosphatidylserine exposure. *Cytometry 31:1.*
54. Kayalar, C., T. Ord, M. P. Testa, L. T. Zhong, and D. E. Bredesen. 1996. Cleavage of actin by interleukin 1β-converting enzyme to reverse DNase I inhibition. *Proc. Natl. Acad. Sci. USA 93:2234.*
55. Kerr, J. F. R., and B. V. Harmon. 1991. Apoptosis: the molecular basis of cell death. In *Definition and Incidence of Apoptosis: An Historical Perspective*, Vol. 3. L. D. Tomei and F. O. Cope, eds. Cold Spring Harbor Lab. Press, Cold Spring Harbor, p. 5.
56. Spano, A., L. Sciola, G. Monaco, and S. Barni. 2000. Relationship between actin microfilaments and plasma membrane changes during apoptosis of neoplastic cell lines in different culture conditions. *Eur. J. Histochem. 44:255.*
57. Naito, Y., K. Saito, K. Shiiba, A. Ochuchi, K. Saigenji, H. Nagura, and H. Ohtani. 1998. $CD8^+$ T cells infiltrated within cancer cell nests as a prognostic factor in human colorectal cancer. *Cancer Res. 58:3491.*
58. Jacquemier, J., F. Eisinger, C. Nogues, Z. Z. Sun, J. M. Guinebretiere, J. P. Peyrat, J. Geneix, R. Lidereau, D. Birnbaum, and H. Sobol. 1999. Histological type and syncytial growth pattern affect E-cadherin expression in a multifactorial analysis of a combined panel of sporadic and BRCA1-associated breast cancers. *Int. J. Cancer 83:45.*
59. Grunwald, G. B. 1993. The structural and functional analysis of cadherin calcium-dependent cell adhesion molecules. *Curr. Opin. Cell. Biol. 5:797.*
60. Takeichi, M. 1991. Cadherin cell adhesion receptors as morphogenetic regulator. *Science 251:1451.*
61. Eisinger, F., C. Nogues, D. Birnbaum, J. Jacquemier, and H. Sobol. 1998. BRCA1 and medullary breast cancer. *JAMA 280:1227.*
62. Eisinger, F., J. Jacquemier, C. Charpin, D. Stoppa-Lyonnet, B. Bressac-de Paillerets, J. P. Peyrat, M. Longy, J. M. Guinebretiere, R. Sauvan, T. Noguchi, et al. 1998. Mutations at BRCA1: the medullary breast carcinoma revisited. *Cancer Res. 58: 1588.*
63. Casiola-Rosen, L., F. Andrade, D. Ulanet, W. F. Wong, and A. Rosen. 1999. Cleavage by granzyme B is strongly predictive of autoantigen status: implications for initiation of autoimmunity. *J. Exp. Med. 190:815.*
64. Darmon, A. J., D. W. Nicholson, and R. C. Bleackley. 1995. Activation of the apoptotic protease CPP32 by cytotoxic T-cell-derived granzyme B. *Nature 377:446.*
65. Casiola-Rosen, L., A. Rosen, M. Petri, and M. Schlissel. 1996. Surface blebs on apoptotic cells are sites of enhanced procoagulant activity: implications for coagulation events and antigenic spread in systemic lupus erythematosus. *Proc. Natl. Acad. Sci. USA 93:1624.*
66. Casciola-Rosen, L. A., G. Anhalt, and A. Rosen. 1994. Autoantigens targeted in systemic lupus erythematosus are clustered in two populations of surface structures on apoptotic keratinocytes. *J. Exp. Med. 179:1317.*
67. Gilligan, H. M., B. Bredy, H. R. Brady, M. J. Hebert, H. S. Slayter, Y. Xu, J. Rauch, M. A. Shia, J. S. Koh, and J. S. Levine. 1996. Antineutrophil cytoplasmic autoantibodies interact with primary granule constituents on the surface of apoptotic neutrophils in the absence of neutrophil priming. *J. Exp. Med. 184:2231.*
68. Konstandoulakis, M. M., K. N. Syrigos, M. Leandros, A. Charalabopoulos, A. Manouras, and B. C. Golematis. 1998. Autoantibodies in the serum of patients with gastric cancer: their prognostic importance. *Hybridoma 17:431.*
69. Ronai, Z., and D. Sulitzeanu. 1986. (Auto)antibodies in human breast cancer sera against antigens associated with breast cancer cells, detected by immunoblotting. *J. Natl. Cancer Inst. 77:1203.*
70. Lenner, P., F. Wiklund, S. O. Emdin, C. Arnerlöv, C. Eklund, G. Hallmans, H. Zentgraf, and J. Dillner. 1999. Serum antibodies against p53 in relation to cancer risk and prognosis in breast cancer: a population-based epidemiological study. *Br. J. Cancer 79:927.*
71. Tang, R., M. C. Ko, J. Y. Wang, C. R. Changehien, H. H. Chen, J. S. Chen, K. C. Hsu, J. M. Chiang, and L. L. Hsieh. 2001. Humoral response to p53 in human colorectal tumors: a prospective study of 1,209 patients. *Int. J. Cancer 94:859.*
72. Metcalfe, S., T. K. Wheeler, S. Picken, S. Negus, and A. Jo Milner. 2000. P53 autoantibodies in 1006 patients followed up for breast cancer. *Breast Cancer Res. 2:438.*